

Modeling saline fluid flow through subglacial ice-walled channels and the impact of density on fluid flux

Amy Jenson^{1,2}, Mark Skidmore³, Lucas Beem³, Martin Truffer², and Scott McCalla¹

¹Department of Mathematical Sciences, Montana State University, Bozeman, Montana, USA

²Geophysical Institute, University of Alaska Fairbanks, Fairbanks, AK, USA

³Department of Earth Sciences, Montana State University, Bozeman, Montana, USA

Correspondence: Amy Jenson (ajjenson@alaska.edu)

Abstract. Subglacial hydrological systems have impacts on ice dynamics, as well as, nutrient and sediment transport. There has been extensive effort to understand the dynamics of subglacial drainage through numerical modeling. These models, however, have focused on freshwater in warm ice and neglected the consideration of fluid chemistry such as salts. Saline fluid can exist in cold-based glacier systems where freshwater cannot and understanding the routing of saline fluid is important for understanding geochemical and microbiological processes in these saline cryospheric habitats. A better characterization of such terrestrial environments may provide insight to analogous systems on other planetary bodies. We present a model of channelized drainage from a hypersaline subglacial lake and highlight the impact of salinity on melt rates in an ice-walled channel. The model results show that [given a subglacial system at the salinity-dependent melting point](#), channel walls grow more quickly when fluid contains higher salt concentrations which lead to higher discharge rates. We show this is due to a higher density fluid moving through a gravitational potential [which generates more energy for melting](#). This model provides a framework to assess the impact of fluid chemistry and properties on the spatial and temporal variation of fluid flux.

1 Introduction

Subglacial hydrology is of fundamental importance to the dynamics and evolution of ice masses (Flowers, 2018; Morlighem et al., 2014). The presence, distribution, and geometry of the subglacial water system have direct effects on rates of ice sliding, ice mass flux, erosion, and deposition (Russell et al., 2006; Bell et al., 2007; Stearns et al., 2008; Siegfried et al., 2016; Larsen and Lamb, 2016; Seroussi et al., 2017; Carrivick et al., 2018). The subglacial hydrological system affects the distribution and character of subglacial biological communities and influences water and nutrient flux into surrounding water bodies (Neal, 2007; Kjeldsen et al., 2014; Meerhoff et al., 2019; Mikucki et al., 2004; Vick-Majors et al., 2020). Whether the goal is to project future sea level rise, understand glacier bed forms, model ocean circulation, or to investigate extra-planetary life through Earth analogs, we require an understanding of the distribution and dynamics of subglacial hydrological systems (Nienow et al., 2017; Forte et al., 2016) (e.g. Nienow et al., 2017; Forte et al., 2016).

Subglacial lakes have been observed to drain episodically through outburst floods and less catastrophically through longer-lived drainage events. There is a significant body of work on modeling the drainage of glacial lakes (Rothlisberger, 1972; Nye, 1976; Spring

25 [\(e.g. Rothlisberger, 1972; Nye, 1976; Spring and Hutter, 1981; Fowler, 1999; Clarke, 2003; Evatt et al., 2006; Kingslake, 2015; Schoof, 2015\)](#). Many subglacial hydrology models have assumed that drainage from a subglacial lake occurs through ice-walled channels at the ice-bed interface [\(Nye, 1976; Fowler, 1999; Clarke, 2003; Evatt et al., 2006\)](#) [\(e.g. Nye, 1976; Fowler, 1999; Clarke, 2003; Evatt et al., 2006\)](#). This work has focused on freshwater at the pressure melting point and neglected the consideration of water chemistry.

The chemistry of the subglacial water influences the character of the hydrological system. Depression of the pressure melting point through increased solute concentration is one potential mechanism to explain the presence of subglacial water in locations with a subglacial temperature below, sometimes significantly below, the pressure melting point (Mikucki et al., 2015). Locations with observable saline discharge occur in both Antarctic and Arctic settings such as Blood Falls, Taylor Glacier, East Antarctica and Borup Fiord Pass Glacier, Ellesmere Island Canada (Trivedi et al., 2018; Lyons et al., 2019). The salinity of the englacial brine feeding Blood Falls is approximately 125 psu but the precise geometry of the subglacial brine system beneath Taylor Glacier is not fully understood (Badgeley et al., 2017; Lyons et al., 2019). Hubbard et al. (2004) inferred that a zone 3-6 km upglacier from the terminus contained saturated sediments or ponded water, based on radar data, and widespread hypersaline groundwater has been detected as far as 5.7 km upglacier from the terminus using transient electromagnetic techniques (Mikucki et al., 2015). Hypersaline lakes have been inferred to exist beneath the Devon Ice Cap, Canadian high Arctic from airborne radio echo sounding data, with predicted salinity in the range of 140 to 160 psu (Rutishauser et al., 2018). However, the effects of increased salinity on the geometry and flow in subglacial hydrological systems remains unknown.

Subglacial water chemistry is expected to impact the geometry and dynamics of the subglacial hydrological system. For instance, the hydraulic potential field is modified through the density of the fluid; saline fluid can have a significantly different flow path than freshwater for the same glacier geometry (Badgeley et al., 2017; Rutishauser et al., 2022). The size and edge dynamics for a channel are also expected to differ as the result of fluid chemistry.

45 An understanding of the impact fluid chemistry has on subglacial systems is important for mapping and classifying subglacial hydrological features using radar. The size, continuity, and electrical conductivity of subglacial channels determines the detectability of subglacial features by radar remote sensing. Constraints provided by modelling inform radar system design decisions such as power requirements, center frequency, and antenna geometry (Scanlan et al., 2022). The ongoing development of multi-polarization radar system and radar processing algorithms increases the detectability of variations in subglacial hydrological organization. The expected geometry of subglacial features is an important specification for the design of radar system. The response in the geometry of subglacial features to changes in the discharge, position along glacier flow, and aqueous chemistry provides constraints for the technological and scientific development of new radar systems.

Basal thermal regimes have been shown to impact the solutes, nutrients, and microbes found in the subglacial systems (Dubnick et al., 2020) and subglacial fluid flow can transport these materials leading to a change in the geomicrobiology of local and nearby environments (Mikucki et al., 2004). We hypothesize that both the basal thermal regime and solute concentrations influence the subglacial hydrological system by altering the effective pressure and fluid flux (which in turn will influence geomicrobiology). A better understanding of the flow dynamics in cold ice is important for characterizing the distinct biogeochemistry in saline subglacial systems.

Table 1. List of model parameters [and variables](#). Values of constants are specified in brackets.

Variable	Description
ρ_i, ρ_w, ρ_b	densities of ice [917 kg m ⁻³], water [997 kg m ⁻³], and brine
g	gravitational acceleration [9.81 m s ⁻²]
\mathcal{L}, σ_i	latent heat of fusion [3.34 x 10 ⁵ J kg ⁻¹] and specific heat capacity for ice [2093 J kg ⁻¹ C ⁻¹]
A, n	ice flow law parameter and exponent [3]
K	ice flow parameter for conduit closure
f, \mathcal{R}, n_i, n_b	friction factor, hydraulic roughness, and roughness of ice [0.6 m ^{-1/3} s] and bed material [0.16 m ⁻¹]
x, s	horizontal and bed-parallel spatial coordinates
B, L	bed slope [3° C], channel length
Q, m	discharge along the conduit and melt rate
S, r	cross-sectional area and channel radius
P_i, ψ	ice overburden pressure and basic hydraulic gradient
N	effective pressure
h, h_i	lake depth and initial lake depth
H	ice thickness from surface to bed adjacent lake
p coefficient describing lake hypsometry V, V_i	volume of lake and initial volume of lake
$\theta_i, \theta_w, \theta_b$	temperatures of basal ice, water, and brine
$\hat{\theta}_w, \hat{\theta}_b$	freezing point of water and brine at pressure
$\hat{\theta}$	salinity- and pressure-dependent melting point of ice
$\beta, \hat{\beta}$	salt concentration in psu and kg m ⁻³

By modeling saline fluid flow through cold ice, we seek to address the following questions: how significant is the effect of salinity on channel wall melt rates; how does the salt concentration change along the channel in response to the melting of the channel walls; and in what systems is the consideration of fluid chemistry and fluid properties important for understanding subglacial hydrology. To answer these questions, we mathematically investigate channel evolution, effective pressure, and discharge over time in response to variable fluid chemistry. The results show that the radius of an evolved channel is larger for saline fluid than the fresh water equivalent ~~-, which affects~~ [when both glacier-lake systems are at their respective salinity and pressure-dependent melting points. The larger channel cross-sections affect](#) the temporal and spatial evolution of fluid flux [for saline fluid](#). This effect is of leading order for gravity driven fluid flow, due to the energy generated when a higher density fluid moves through a gravitational potential. We find that the same result occurs for high density freshwater such as water carrying high loads of suspended sediment. The ~~difference between fluid chemistry is~~ [differences related to fluid chemistry are](#) greatest for high discharge rates which are generated by high volume lakes and channels with steep bed slopes and circular geometry.

70 2 Model description

2.1 Model equations

~~Building on the model developed by Nye (1976) and adapted by~~ We construct a lake-drainage model in which the water flows from a subglacial lake through an R-channel (Rothlisberger, 1972; Nye, 1976). We follow the implementation and notation of Fowler (1999) and Kingslake (2015). ~~In our model,~~ we assume a subglacial conduit on an inclined bed slope beneath ice of constant thickness τ (Fig. 1). In contrast with these previous approaches, we allow for varying salt concentrations in fluid flowing from a subglacial lake. The ice and fluid are assumed to be at the salinity- and pressure-dependent melting point of the fluid. For a list of model ~~parameters and variables and parameters along with the consistently used parameter~~ values see Table 1.

The ~~negative~~ basic hydraulic gradient ~~was defined by Fowler (1999) as is~~ the sum of the glacier geometry related terms,

$$80 \quad \psi = \rho_b g \sin B - \frac{\partial P_i}{\partial s}, \quad (1)$$

where B is the conduit slope (assumed to be constant along the channel and the same as the bed slope), s is the along-flow coordinate parallel to the bed, and g is gravitational acceleration (Fowler, 1999). The ice-overburden pressure P_i in [Pa] is given by $P_i = \rho_i g H$ where H is the glacier thickness. Since we assume the ice thickness is constant, the change in ice-overburden pressure along the channel is zero ~~and $\psi = \rho_b g \sin B$.~~ The total ~~negative~~ potential gradient is ~~given by-~~

$$85 \quad G = \psi + \frac{\partial N}{\partial s}, \quad (2)$$

where N is the effective pressure which is the difference between the ice-overburden pressure and the water pressure in the channel.

We assume a channel already exists and the channel walls open due to melt and close due to creep closure. Together these govern the rate of change of the conduit cross-sectional area S with respect to time t ,

$$90 \quad \frac{\partial S}{\partial t} = \frac{m}{\rho_i} - K S N^n, \quad (3)$$

where m is the melt rate in [$\text{kg m}^{-1} \text{s}^{-1}$] and $K = 2A/(n^n)$ is a function of the Glen's flow law parameter A and exponent n (Evatt et al., 2006). We calculate A as a function of ice temperature using the Arrhenius relation and relevant calibrated values (Cuffey and Paterson, 2010, Eqn 3.35).

Mass conservation relates the rate of change of conduit area to the spatial gradient in discharge Q , the production of water due to melt, and additional water added to the system along the conduit, such that

$$95 \quad \frac{\partial S}{\partial t} + \frac{\partial Q}{\partial s} = \frac{m}{\rho_b}. \quad (4)$$

We assume turbulent flow and use Manning's formula to empirically relate the total potential hydraulic gradient (basic hydraulic gradient and the effective pressure gradient) to friction along the channel. Note that Manning's formula was derived

for freshwater, but due to a lack of empirical data with saline fluid in ice, we use the Manning's friction factor for freshwater
 100 in ice used in Fowler (1999) ~~(instead of Darcy-Weisbach)~~. The conservation of momentum equation is then,

$$\psi + \frac{\partial N}{\partial s} = f \rho_b g \frac{Q|Q|}{S^{8/3}}, \quad (5)$$

where f is the friction factor. For a circular ice-walled channel, $f = (4\pi)^{2/3} \mathcal{R}^2$ and ~~$\mathcal{R} = n_i = 0.6$~~ $\mathcal{R} = n_i = 0.06$ $\text{m}^{-1/3}$ s
 where \mathcal{R} is the hydraulic roughness and n_i is the roughness of ice [Clarke \(2003\)](#). For a semi-circular channel at the bed,
 $f = (2(\pi + 2)^2 \pi)^{2/3} \mathcal{R}^2$ where $\mathcal{R} = \pi/(2 + \pi)n_i + (1 - (\pi/(2 + \pi)))n_b$ and $n_b = 0.16 \text{ m}^{-1/3}$ s is the roughness of the bed
 105 material (Fowler, 1999, Eq. 2.24).

As brine flows through the channel, the viscous dissipation of heat causes melting along the channel walls and results in
 dilution of the brine. The salinity, or salt concentration, of the brine ~~is therefore non-constant~~ therefore varies along the channel
 in time. We derive an equation describing the evolution of the concentration of the salt (see details in Sec.2.2). Due to changing
 salt concentrations, the density of brine and the melting point of ice also vary spatially and temporally. The density of the
 110 brine in $[\text{kg m}^{-3}]$ as a function of salt concentration β in psu-practical salinity units [psu] under 1 bar using the FREezing
 CHEMistry (FREZCHEM) model from Wolfenbarger et al. (2022) results in

$$\rho_b(\beta) = 9.97809.98 \times 10^{-10-7} \beta^3 + 5.53285.53 \times 10^{-8-5} \beta^2 + 7.63467.63 \times 10^{-4-1} \beta + 9.99841.00 \times 10^{-13}. \quad (6)$$

~~where density is in kg m^{-3}~~ . Note we do not account for changes in density due to pressure. Using the same FREZCHEM
 model, we calculate the ~~change in the~~ melting point of ice due to salinity and adjust for the ~~change in ice-overburden~~ pressure
 115 (Chang et al., 2022). The melting point ~~depression in $[\text{°C}]$~~ of ice in contact with saline fluid ~~under 1 bar is~~

$$\underline{\Delta \hat{\theta}_\beta = -5.8202 \times 10^{-7} \beta^3 + 1.8653 \times 10^{-6} \beta^2 - 6.0536 \times 10^{-2} \beta + 2.5195 \times 10^{-3}.$$

~~The change in the melting point due to pressure is~~

$$\underline{\Delta \hat{\theta}_P = 1.7628 \times 10^{-26} P_i^3 - 1.5226 \times 10^{-16} P_i^2 - 7.4477 \times 10^{-8} P_i + 1.1645 \times 10^{-2},$$

~~where at pressure P_i is the ice-overburden pressure in bars. The adjusted pressure and salinity dependent melting point is then~~

$$120 \quad \underline{\hat{\theta} = \Delta \hat{\theta}_P + \Delta \hat{\theta}_\beta.$$

$$\underline{\hat{\theta} = -5.81 \times 10^{-7} \beta^3 + 1.24 \times 10^{-6} \beta^2 - 6.05 \times 10^{-2} \beta - 7.45 \times 10^{-8} P_i. \quad (7)$$

We ~~set the ice and brine temperature~~ assume the lake and surrounding ice system is in thermal equilibrium which requires
~~that at the lake, the ice and brine temperatures, θ_i , and θ_b , respectively, equal to the melting point of ice are equal and at~~
 125 the salinity and pressure-dependent melting point $\hat{\theta}$ at time zero and assume the brine temperature is constant. For a given
salt concentration in the lake, we calculate the melting point at the lake and set the ice and brine temperatures equal to that

temperature. We assume the ice and brine temperatures remain constant in time and along the channel; this is realistic for most freshwater systems (Clarke, 2003). However, the melting point only remains constant at the lake and evolves in response to the changes in salinity along the channel and in time. With these assumptions, the conservation of energy equation is

$$130 \quad Q \left(\psi + \frac{\partial N}{\partial s} \right) = m\mathcal{L} + m\sigma_i(\hat{\theta} - \theta_i), \quad (8)$$

where σ_i is the specific heat capacity of ice and L is the latent heat of fusion for ice. The term on the left hand side of Eq. 8 is the total work done which must be balanced by the sum of the energy lost to melting due to latent heat and lost to raising the ice temperature to the changing melting point. Therefore the amount of energy available for melting the channel walls is a function of salinity. Following Nye (1976) and Kingslake (2015) Rothlisberger (1972) and Nye (1976), we neglect the heat
135 transfer equation which is equivalent to assuming any heat generated from flow is instantaneously transferred to the channel walls.

We assume a circular channel for most simulations, but we do compare the effect of circular vs semi-circular channels in Sec. 3. The main differences between these assumptions are that in the semi-circular case (1) the fluid is flowing along the bed and therefore the roughness of the bed must be accounted for instead of the roughness of ice and (2) the substrate may contain
140 some salts. We do not account for (2) in our model. We do account for (1) through the friction factor which appears in the conservation of energy equation and changes depending on the channel geometry and roughness of the channel walls or the bed.

2.2 Consideration of brine

As the brine flows from the subglacial lake, it will be diluted as meltwater is added along the channel length. To account for
145 this, we have developed a partial differential equation describing the concentration of salt $\hat{\beta}$ [kg m⁻³] at position s and time t . The fluid is moving along the channel at velocity v which gives the flux of salts

$$\phi = v\hat{\beta} - D\frac{\partial\hat{\beta}}{\partial s}$$

where D is the diffusion coefficient. The mean velocity of the fluid is given by $v = Q/S$. We calculate a Péclet number of
150 $(Pe) > 10^8$ which suggests advection dominates diffusion in fluid flow and assume diffusion is negligible. With this assumption, the flux equation becomes

$$\phi = \frac{Q\hat{\beta}}{S}.$$

~~Following the standard derivation for scalar conservation (e.g. Knobel, 2000, Chapter 15), we derive an equation for the evolution of the salt concentration. Assuming there is no brine added along the channel and there is no accretion of brine on the channel walls, there is no source or sink for salt. Under these assumptions, the conservation of mass for $\hat{\beta}$ requires-~~

$$155 \quad \frac{\partial}{\partial t} \int_s^{s+\Delta s} \hat{\beta} S ds = \frac{\partial}{\partial s} \int_s^{s+\Delta s} -\phi S ds.$$

which gives the partial differential equation the salt concentration equation is,

$$\frac{\partial}{\partial t} (\hat{\beta}S) = \frac{\partial}{\partial s} (-Q\hat{\beta}). \quad (9)$$

In the case of a semi-circular channel, contact with the ground could be a source for salts in the fluid flow. Although we do not include it here, such a mechanism could be accounted for in our model as a source term in Eq. 9.

160 The salinity in the lake $\hat{\beta}_0$ salt concentration $\hat{\beta}$ discussed above is in $[\text{kg m}^{-3}]$ in order to be compatible with the model. These values for salinity are converted to a standard unit for measuring salinity [psu] before calculating the density and melting point in Eqs. 6 and 7 respectively using the conversion $\hat{\beta} [\text{kg m}^{-3}] = 1000\beta(\rho_b)^{-1} [\text{psu}]$. The salinity in the lake is constant in time since no fluid is being added to the lake which gives the boundary condition $\hat{\beta}(0,t) = \hat{\beta}_0\hat{\beta}(0,t) = 1000\beta(0,t)(\rho_b)^{-1}$ where $\beta(0,t)$ in [psu] is prescribed at the beginning of the simulation. When the cross-sectional area of the channel is small,

165 there is less melting and the dilution of the brine is minimal so at the beginning of the simulation we assume that the salt concentration in channel is equal to the concentration in the lake, that is $\hat{\beta}(s,0) = \hat{\beta}_0\hat{\beta}(s,0) = \hat{\beta}(0,t)$.

2.3 Channel boundary conditions

The only fluid flux from the subglacial lake is the brine flowing out of the channel. Thus the rate of change of lake volume V is given by

$$170 \quad \frac{dV}{dt} = -Q(0,t). \quad (10)$$

~~Following Kingslake (2015), we define~~ We assume a box-shaped lake which gives the lake hypsometry by

$$\left(\frac{h}{h_i}\right)^p = \frac{V}{V_i} \quad (11)$$

where h is the depth of the lake, h_i is the initial lake depth, and V_i is the initial lake volume. ~~The dimensionless parameter p depends on lake shape. We assume a box-shaped lake where $p=1$. For the treatment of more complicated lake geometries, see~~

175 Kingslake (2013).

Implicitly differentiating gives

$$\frac{dV}{dt} = \frac{dV}{dh} \frac{dh}{dt} = \frac{h^{p-1} V_i}{h_i} \frac{dh}{dt} \quad (12)$$

and by substitution, the lake depth evolves with time following

$$\frac{dh}{dt} = \frac{h_i}{V_i} (-Q(0,t)). \quad (13)$$

180 We assume the lake drains slowly enough that the ice roof drops with the lake depth following Evatt et al. (2006), so the effective pressure is the difference between the ice overburden pressure and the fluid pressure in the lake. The boundary condition where the conduit meets the lake is ~~$N_L = N(0,t) = 0$~~ $N(0,t) = 0$ (Evatt et al., 2006). We ~~do not require the channel~~

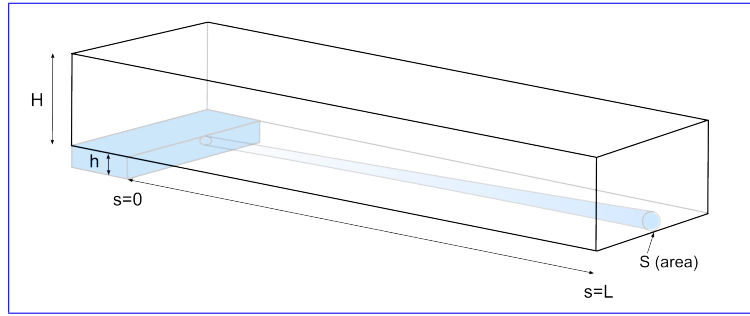


Figure 1. Schematic of simple glacier geometry and subglacial hydrological system with an R-channel draining a subglacial lake.

~~to exit at a terminus or end subaerially and so we impose a no flux~~ impose a Neumann boundary condition at the end of the channel where

$$185 \quad \left. \frac{\partial N(s, t)}{\partial s} \right|_{s=L} = 0. \quad (14)$$

We choose this boundary condition (opposed to $N = 0$) in order to solve the system numerically in a more efficient way (see Appendix A and Sec. 4.4). Neumann boundary conditions on effective pressure at the end of the channel have been used to solve similar systems of equations without an influence on the qualitative results (Kingslake, 2015; Evatt et al., 2006).

The ~~model equations coupled with our salt concentration equation and~~ full model contains five unknowns ($N, S, m, Q,$ and β) and five model equations (Eqs. 3, 4, 5, 8, and 9) which are solved simultaneously. The model equations contain the derived variables $\hat{\theta}, \rho_b,$ and ψ which depend on salinity. The model equations written in terms of the salinity-dependent parameters derived variables are listed below.

Summary of model equations

$$195 \quad \begin{aligned} \text{Channel evolution: } \frac{\partial S}{\partial t} &= \frac{m}{\rho_i} - KSN^3 & \text{Conservation of mass: } \frac{\partial S}{\partial t} + \frac{\partial Q}{\partial s} &= \frac{m}{\rho_b} \\ \text{Conservation of momentum: } \psi + \frac{\partial N}{\partial s} &= f\rho_b g \frac{Q^2}{S^{8/3}} & \text{Conservation of energy: } m\mathcal{L} + m\sigma_i(\hat{\theta} - \theta_i) &= Q \left(\psi + \frac{\partial N}{\partial s} \right) \\ \text{Salt Concentration: } \frac{\partial}{\partial t} (\hat{\beta}S) &= \frac{\partial}{\partial s} (-Q\hat{\beta}) \end{aligned}$$

200 These five equations are non-dimensionalized and solved numerically as described in Appendix ??-A. The system of equations are solved using a constant time step of approximately 3 seconds and a constant grid spacing of 20 m. After the solution to the salt concentration equation is obtained at each time and space step, the melting point $\hat{\theta}$, and the density ρ_b are updated along with the basic hydraulic gradient ψ , which is a function of density using Eqs. 7, 6, 1 respectively.

3 Results

Idealized model simulations were run to investigate the impact of brine on discharge rates, channel radius, effective pressure, and the duration of lake drainage. The model runs until open channel flow occurs, at which point the model run ends. Unless

otherwise specified, the parameters used for the baseline simulations are as follows: ice thickness above channel $H = 100$ m, 205 initial lake volume $V_i = 1 \times 10^6 \text{ m}^3$, initial lake depth $h_i = 10$ m, channel length $s = 1000$ m, initial channel radius $r = 0.25$ m, bed and conduit slope $B = 3^\circ$, and circular channel geometry. A range of different values were explored for each parameter listed in Table 2 while holding all other parameters equal to the baseline simulation values.

To investigate the effect of saline fluid, we ran five scenarios with ~~$\beta = \{0, 50, 100, 150, 200\}$~~ $\beta = \{0, 50, 100, 150, 200 \text{ psu}\}$ to explore the range of possible outcomes. The discharge rates are greater for fluid with higher salt concentrations (Fig. 2a). 210 Early in the simulations, the discharges at the lake are nearly equal for all salinities. Later on there is a greater difference in discharge rates. Higher salt concentrations increases the peak velocity reached and decreases the amount of time to reach peak velocity (Fig. 2b). The peak velocity and drainage duration change nearly linearly with increased salt concentrations. The channel radius increases slightly along the channel for all scenarios (Fig. 2c) and at the end of the simulations after the lake has drained, the channel radius is greater for the higher salt concentrations.

215 The difference between the channel salt concentration after the lake has emptied and the initial salt concentrations is small for all scenarios (Fig. 2d). However greater dilution occurs in the channels with higher salinity and therefore greater fluid flux.

We systematically vary parameters to explore the sensitivity of the model and the impact of channel geometry, lake volume, initial channel radius, and bed slope on discharge and the duration of drainage (Fig. 3). The channel geometry (circular vs. semi-circular) changes the time of lake drainage, as well as the peak discharge for freshwater and for a lake with salinity of 220 100 psu (Fig. 3a). For a semi-circular channel, the difference in time until lake drainage is more significant than the difference in peak discharge between the freshwater and brine scenarios. For the circular channel, the difference in peak discharge is greater than the difference in the duration of time until lake drainage. In both scenarios, the circular channel drains the lake in less than half the time than for a semi-circular channel and the peak discharge is about twice as high when the channels are circular. This is because the initial cross sectional area is doubled for those simulations.

225 The volume of the lake impacts the discharge and the timing of drainage by extending the amount of time the model is run (Fig. 3b). The discharge curves for all lake volumes follow the same curve until the smaller lakes drain. The lake continues to drain for greater lake volumes and the peak discharge increases by two orders of magnitude when comparing $V_i = 1 \times 10^5 \text{ m}^3$ and $V_i = 1 \times 10^7 \text{ m}^3$.

For smaller channels ($r < 0.25$ m), the initial channel radius impacts the amount of time until the lake drains but does not 230 change the peak discharge reached (Fig. 3c). The channels with smaller initial radius take longer to reach peak discharge. For larger initial channel radius ($r > 0.25$ m), both timing and peak discharge are impacted by an increase in radius, where larger channels tend to reach higher peak discharges in less time. Increasing the bed and channel slope increases the peak discharge and decreases the time to reach that peak (Fig. 3d). We varied fresh water ($\beta = 0$ psu) and brine ($\beta = 100$ psu) along with the channel slope and found that for lower slopes there is a larger difference in timing between brine and freshwater and for greater 235 slope there is a larger difference in peak discharge between brine and freshwater. Higher bed slopes lead to higher discharge rates more quickly (Fig. 3d).

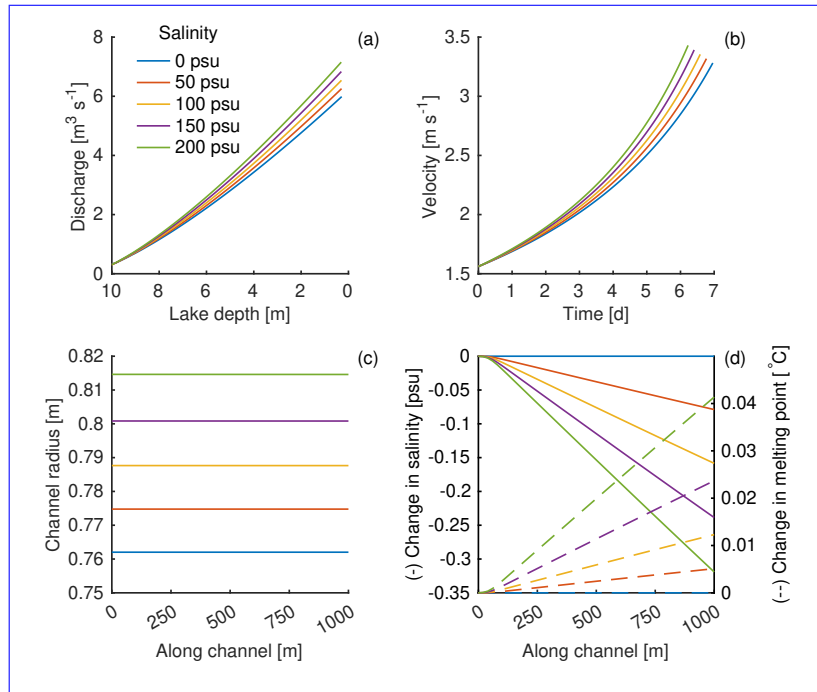


Figure 2. The impact of brine on discharge, velocity, channel radius, salt concentration, and effective pressure for various initial salt concentrations, shown by the colors in (a). (a) Discharge at the lake outlet as the lake drains. (b) Velocity at the lake outlet over time in days. (c) Channel radius along the length of the channel at the time the lake has emptied. (d) The solid lines are associated with the left axis which is the difference between the final salt concentration after the lake has emptied and the initial salt concentrations shown in the legend of (a) along the channel. The right axis (dashed lines) refers to the difference between the melting points at the end of the simulation along the channel and the initial melting point, where the change in the melting point is only due to the change in the salinity (shown in the left axis).

We explored lake depths of 5 – 15 m, ice thicknesses of 100 – 1000 m, and channel lengths of 500 – 5000 m and found that these parameters do not substantially impact the results for the parameter combinations described. For a list of parameters and the range of values explored, see Table 2.

240 As the walls of the channel melt and the brine is diluted, the properties of the brine, such as specific heat capacity and density, change. We have accounted for these changes in our simulations, but neglecting these changes in brine properties does not have a substantial influence on the results.

4 Discussion

245 The results of this model suggest that the consideration of brine in relevant glacial systems is important for capturing the dynamics of drainage through ice-walled channels: a failure to include brine leads to substantially different estimates on channel formation and drainage timescales (Fig. 2). The consideration of brine is more important when considering systems

Table 2. Prescribed model parameter variables and descriptions with baseline simulation values and ranges explored.

Variable	Description	Baseline	Range
s	length of channel	1000 m	[500 – 5000 m]
B	bed (conduit) slope	3°	[$2 - 4^\circ$]
r	initial channel radius	0.25 m	[0.1 – 0.5 m]
h	initial lake depth	10 m	[5 – 15 m]
H	ice thickness above bed and channel	100 m	[100 – 1000 m]
V_i	reference volume of lake	$1 \times 10^6 \text{ m}^3$	[$1 \times 10^5 - 1 \times 10^7 \text{ m}^3$]
β	salt concentration of brine in lake	0, 100 psu	[0 – 200 psu]

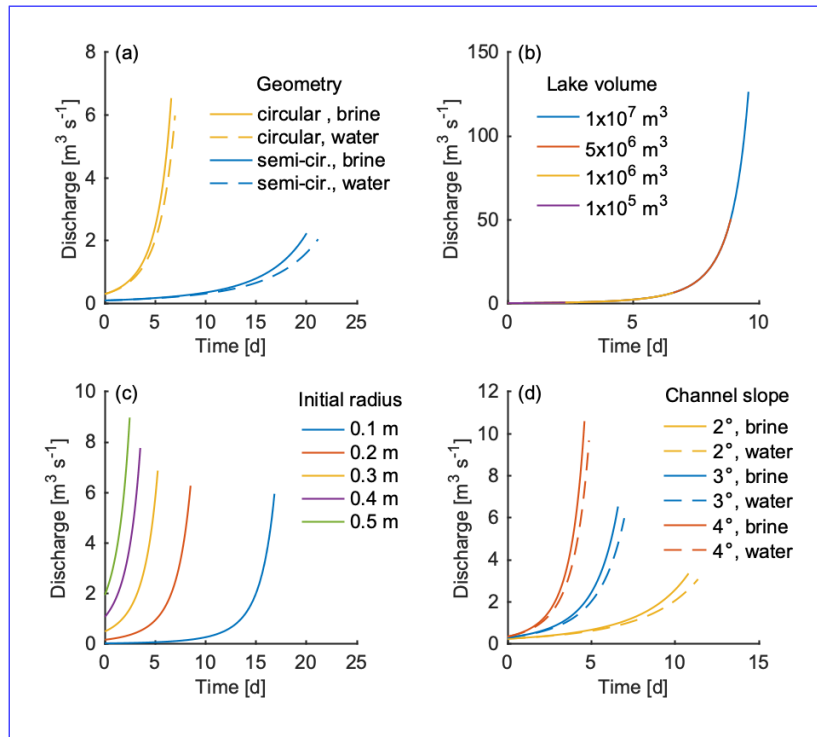


Figure 3. Discharge over time for different channel geometries, lake volumes, initial channel radius, and channel (bed) slope. (a) A channel with semi-circular geometry for a lake with salinity 0 psu (dashed line) and 100 psu (solid line) are denoted in blue. A circular channel geometry for a lake with salinity 0 psu (dashed line) and 100 psu (solid line) are denoted in yellow. (b) Lake volumes for $V_i = 1 \times 10^7 \text{ m}^3$ (blue line), $V_i = 5 \times 10^6 \text{ m}^3$ (red line), $V_i = 1 \times 10^6 \text{ m}^3$ (yellow line), and $V_i = 1 \times 10^5 \text{ m}^3$ (purple line) are plotted over top of one another for a lake with salinity of 100 psu. (c) The initial channel radius from a lake with salinity of 100 psu is varied such that the blue line is $r = 0.1 \text{ m}$, the red line is $r = 0.2 \text{ m}$, the yellow line is $r = 0.3 \text{ m}$, purple line is $r = 0.1 \text{ m}$, and the green line is $r = 0.5 \text{ m}$. Channel slope is varied for 2° (in yellow), 3° (in blue), 4° (in red) for a lake with salinity of 100 psu (solid) and 0 psu (dashed).

with high lake volume and steep bed slopes (Fig. 3b,d). This is particularly important for gravitationally generated flows where the high density significantly increases fluid flow rate. Large circular channels also tend to lead to more dramatic differences in the fluid dynamics between high and low concentrations of salt (Fig. 3a,c).

250 4.1 Density, a first order effect

In our model for the parameters we explored, density is the leading order effect of salinity on the fluid dynamics. A fluid with higher salt concentrations has a higher density. As the denser material moves through the gravitational potential, more energy is available for melting. The observed higher discharge for higher salinity systems results from the increased density. In Fig. 4a, fresh water is modeled with varying densities equivalent to the density of brine with salinities $\beta = 0, 50, 100, 150, 200$. These
255 velocity curves are nearly identical to the curves in Fig. 2b.

The presence of salt in the system tends to ~~decrease~~ increase the amount of energy ~~available for melting as a result of the increase in the melting point of ice, needed to melt the channel walls because the ice temperature must increase to the evolving melting point before melting. As the salinity along the channel changes, the melting point changes and subsequently the energy needed to melt the channel walls,~~ although this change is minimal as seen in Fig. 2d. ~~However, the~~ The latent heat of fusion
260 is far greater than this term and thus any changes in the melting point has little effect on the total energy available for melting and therefore fluid velocities. Modeling all other changes related to salinity (including the treatment of the melting point and fluid temperature) while holding the density of the brine constant and equal to that of fresh water results in the velocities shown in Fig. 4b. ~~Neglecting consideration of brine density results in almost no changes~~ Without the consideration of a change in density, there is almost no change in the velocity curves.

265 It is important to note that the increased density increases melt only when the flow itself is gravity driven (i.e., an downward sloped inclined channel). For example, if the flow of a saline fluid is driven uphill by glacial overburden pressure, the fluid velocity will be slower compared to the fluid velocity of fresh water.

4.2 Outburst floods

Outburst floods often result in disproportionate amounts of suspended sediments which increases the density of the water
270 (Snorrason et al., 2002; Church, 1972). Discharge from outburst floods are typically on the order of $100 - 1000 \text{ m}^3 \text{ s}^{-1}$ (Walder and Costa, 1996, Table 1) and can contain suspended sediment concentrations SSC of up to 70.7 g L^{-1} (Beecroft, 1983; Old et al., 2005) ~~with a lower threshold for hyper-concentrated sediment concentrations of and in some extreme cases~~ over 400 g L^{-1} (Maizels, 1997). The density of sediments ρ_s depends on the rock type and clast size, but typically range from $2350 - 2760 \text{ kg m}^{-3}$ (Frederick et al., 2016; Guan et al., 2015; Chikita, 2004). The combined fluid density ρ_c of water with
275 suspended sediments is related to suspended sediment concentration by,

$$\rho_c = \frac{SSC}{\rho_w} \rho_s + \left(1 - \frac{SSC}{\rho_w}\right) \rho_w. \quad (15)$$

As shown in Sec. 4.1, density has a significant effect on fluid flow regardless of salinity. We model an outburst flood from a subglacial lake with freshwater at 0° C and a volume of $V_i = 1 \times 10^7 \text{ m}^3$ with all other parameters equal to those in the baseline

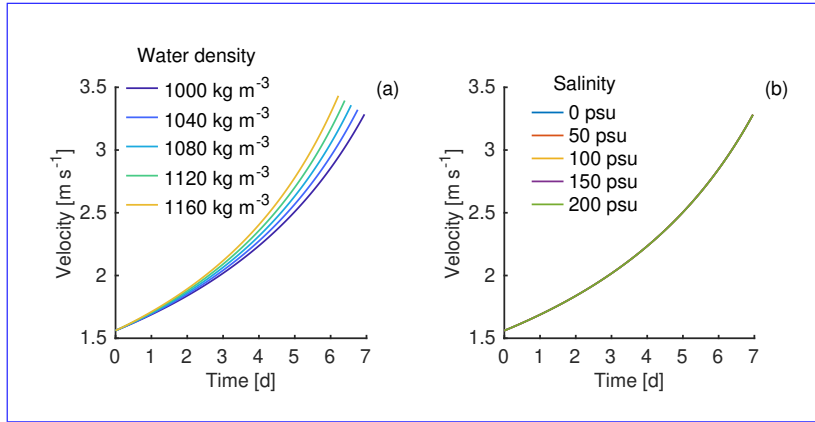


Figure 4. (a) Velocity curves for scenario with fresh water at 0° C with densities equivalent to those of brines with salinities $\beta = 0, 50, 100, 150, 200$ psu. (b) Velocity curves for brine with $\beta = 0, 50, 100, 150, 200$ psu, but all with constant density equal to fresh water (1000 kg m^{-3}).

simulation (Table 2). We vary the suspended sediment concentrations from $SCC = \{0, 23, 45, 68, 91\} \text{ g L}^{-1}$ to arrive at fluid
 280 densities of $\rho = \{1000, 1040, 1080, 1120\} \text{ kg m}^{-3}$ to simulate different suspended sediment loading.

~~There is a~~ As can be seen in Fig. 5, there is a significant difference between the peak discharge of floods with a lower density
 fluid ($Q \approx 115 \text{ m}^3 \text{ s}^{-1}$) than with a higher density fluid ($Q \approx 140 \text{ m}^3 \text{ s}^{-1}$) (Fig-5).

~~We also modeled outburst floods where the ice thickness above the channel was not constant, but varied from 100 m above
 the lake to 0 m at the end of the channel. A decrease in ice thickness away from the lake results in a negative ice-overburden
 285 pressure gradient which drives fluid out of the lake by increasing the basic hydraulic gradient (See Eq. 1). This results in
 higher overall discharge rates, but approximately the same difference in peak discharges when comparing high and low density
 fluids. Therefore, the difference between the peak discharges of different density fluids is smaller compared to the overall peak
 discharges and the influence of density becomes less important. Nonetheless, neglecting to as well as the timing. Neglecting
to account for sediment loading and accurate water densities could lead to inaccurate results when modeling outburst floods
 290 where fluid density drives fluid flow.~~

4.3 A different formulation of the energy equation

Realistically, not all energy generated from the viscous dissipation of heat will go into melting as is assumed in the model. Some
 energy will be used to increase the brine temperature. To address this and evaluate the influence of warming brine temperatures
 on fluid flow, we assume here that the temperature of the brine remains equal to the melting point of the ice ($\theta_b = \hat{\theta}$) which
 295 will increase over time as the brine is diluted. We add a term to the conservation of energy to account for the energy needed to
 warm the mass of fluid per unit length by the change in the brine temperature over time $\frac{\partial \theta_b}{\partial t} = \frac{\partial \hat{\theta}}{\partial t}$ (since $\theta_b = \hat{\theta}$). The updated

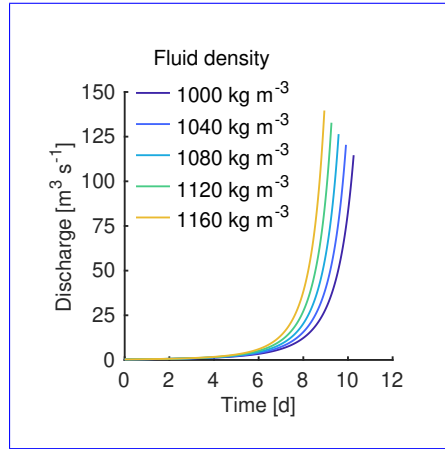


Figure 5. Outburst flood hydrographs for water with different suspended sediment concentrations and therefore varying fluid densities.

conservation equation becomes,

$$m\mathcal{L} + m\sigma_i(\hat{\theta} - \theta_i) + \sigma_b \frac{\partial \hat{\theta}}{\partial t} \rho_b S = Q \left(\psi + \frac{\partial N}{\partial s} \right). \quad (16)$$

The dilution of the brine is minimal (less than 1% for all simulations, see Fig. 2e) and therefore the change in the melting point and brine temperature over time $\frac{\partial \hat{\theta}}{\partial t}$ is small. The energy needed to change the bulk fluid temperature is also minimal, especially in comparison to the latent heat of fusion \mathcal{L} . Considering this term in the energy balance does not significantly influence the results. The difference in discharge between the simulations with and without this additional energy term is on the order of $10^{-3} \text{ m}^3 \text{ s}^{-1}$ and therefore we claim neglecting this term is justified.

4.4 Effective pressures and channel closure

In solving the system of equations, we follow a similar method to that used in Kingslake (2015) and assume that the discharge is constant along the channel (Eq. A9). This is equivalent to assuming the water generated by melting of the channel walls is negligible compared to the flux of fluid from the lake (see Appendix ?? for more details). Additionally, we force the effective pressure gradient to be zero at the end of the channel (Eq. 14), and arrive at an expression for $Q(t)$ that is only a function of the cross-sectional area $S(s=1,t)$ and the basic hydraulic gradient $\psi(s=1,t)$ at the end of the channel over time. As a result, the dimensionless effective pressure gradient can be written as a function of the cross-sectional area and the basic hydraulic gradient both at the end of the channel and along the channel

$$\frac{\partial N}{\partial s} = \frac{1}{\delta} \left(\left(\frac{S(s=1,t) S(1,t)}{S(s,t) S(s,t)} \right)^{8/3} \psi(s=1,t) - \psi(s,t) \right). \quad (17)$$

The cross-sectional area is always smallest at the end of the channel because this is where the melting point is the highest and there is less energy available for melting. This implies that

$$315 \left(\frac{S(s=1,t)}{S(s,t)} \frac{S(1,t)}{S(s,t)} \right)^{8/3} \leq 1 \quad (18)$$

for all (s, t) . Recall the basic hydraulic gradient is a function of fluid density which decreases (very slightly) along the channel as a result of the brine dilution. So the basic hydraulic gradient reaches a minimum at the end of the channel. This causes the effective pressure gradient to be negative (very slightly) for simulations with saline fluid. The effective pressure for all simulations are extremely close to zero ($-200 < N \leq 0$ Pa) and therefore we claim that the sign of the effective pressure is negligible and does not qualitatively affect our results. Physically, this suggests that there is high fluid pressure throughout the channel and there is no channel closure due to ice-overburden pressure. In systems where ice thicknesses are high, this may not be realistic.

5 Conclusions

We have presented a subglacial hydrology model which includes the consideration of saline fluid. Salt allows fluid to exist below the freezing point of freshwater and increases the density of the fluid. We show that if a channel exists, hypersaline fluid can flow through an ice-walled channels at the same subzero temperature channel when the brine and ice are at the salinity and pressure-dependent melting point. Our results suggest that higher salt concentration increases the peak discharge and decreases the duration of time for a fixed volume to drain from a subglacial lake. The main driver of this difference the increased discharge rates as a function of salinity is the higher fluid density -associated with higher salt concentrations. More energy is generated and available for melting the channel walls when a higher density fluid moves through a gravitational potential. While some of this energy is used to warm the ice to the new melting point down the channel as the brine is diluted by meltwater, the melt is minimal compared to the discharge from the lake and therefore does not impact the discharge rates. Aside from the influence of salinity on the depression of the melting point, the greatest difference on fluid flux when considering saline fluids is related to the change in density.

This study shows that accounting for fluid chemistry is crucial for accurately modeling subglacial hydrology in relevant systems (i.e., high density fluid, high lake volumes, steep bed slopes). For a lake with a salinity of 150 psu, which is close to the measured values at Blood Falls (125 psu) and the inferred values at the Devon Ice Cap (140 – 160 psu), the peak discharge reached is 14% greater and the lake drains 10% faster than for a lake with freshwater. The duration of drainage is most sensitive to initial channel radius and channel geometry while peak discharge is most sensitive to lake volume, channel slope, and channel geometry. We explored the influence of varying fluid density related to suspended sediment loads on outburst floods and found that peak discharge is significantly higher for a high density fluid (21% higher than pure water when the fluid density is $1160 \text{ m}^3 \text{ s}^{-1}$). There may be implications for how fluid moves from high pressure, low fluid density systems to high density, low pressure systems and how these interactions change fluid dynamics.

We make a number of simplifying assumptions in the model and use ~~somewhat arbitrary parameters~~ arbitrary parameters for ice thickness, lake volume, channel length, bed slope, and initial channel radius due to a lack of available data on subglacial hypersaline systems. In this light, the model presented here should be viewed as an initial exploration of the impact of brine on the dynamics of a subglacial hydrological system. The model can be used to explore the impact of other solutes on drainage. Additional modeling efforts are needed to provide a thorough sensitivity and stability analysis. Further research is required to understand the initiation of drainage in cold saline environments and the influence of fluid density on drainage networks and outburst floods.

Code availability. MATLAB script files for full model are available at <https://doi.org/10.5281/zenodo.8247882> (Jenson et al., 2023).

Appendix A: ~~Numerical methods~~ Numerics

After non-dimensionalization, the model equations to be solved numerically are the following.

Dimensionless model equations

$$355 \quad \text{Channel Evolution: } \frac{\partial S}{\partial t} = \frac{Q^3}{S^{8/3}(1 + \gamma(\hat{\theta} - \theta_i))} - SN^3, \quad (\text{A1})$$

$$\text{Conservation of Mass: } \frac{\partial Q}{\partial s} = \epsilon(r - 1) \frac{|Q|^3}{S^{8/3}} + \epsilon SN^3, \quad (\text{A2})$$

$$\text{Conservation of Momentum: } \frac{\partial N}{\partial s} = \frac{1}{\delta} \left(\frac{Q^2}{S^{8/3}} - \psi \right), \quad (\text{A3})$$

$$\text{Salt Concentration: } \lambda \frac{\partial}{\partial t} (\hat{\beta} S) = \frac{\partial}{\partial s} (-\hat{\beta} Q), \quad (\text{A4})$$

$$\text{Boundary Conditions: } N_{\underline{L}(0,t)} = 0, \quad (\text{A5})$$

$$360 \quad \left. \frac{\partial}{\partial s} N(s,t) \right|_{s=1} = 0, \quad (\text{A6})$$

$$\hat{\beta}(\underline{0}, t) = \hat{\beta}(0, 0) \quad (\text{A7})$$

$$\frac{dh}{dt} = \zeta Q(0, t). \quad (\text{A8})$$

Model and Scaling Parameters:

$$365 \quad N_0 = (Kt_0)^{-1/3}, \quad m_0 = \frac{Q_0 \psi_0}{\mathcal{L}}, \quad S_0 = \left(\frac{f \rho_b g Q_0^2}{\psi_0} \right)^{3/8}, \quad t_0 = \frac{\rho_i S_0}{m_0},$$

$$r = \frac{\rho_i}{\rho_b}, \quad \epsilon = \frac{s_0 m_0}{Q_0 \rho_i}, \quad \delta = \frac{N_0}{s_0 \psi_0}, \quad \gamma = \frac{\theta_0 \sigma_i}{\mathcal{L}}, \quad \lambda = \frac{S_0 s_0}{t_0 Q_0}, \quad \zeta = \frac{t_0 h_i Q_0}{p V_i h_0}$$

We use the subscripts $j = 1, 2, \dots, n$ to denote the grid points along the channel which are separated by Δs and the superscripts $i = 1, 2, \dots, m$ denote time steps separated by Δt . To solve Eq. (A8), we follow Kingslake (2013) in using the Forward Euler

Method to evolve the lake depth forward in time.

$$h^{i+1} = h^i + \frac{\Delta t \zeta}{(h^i)^{p-1}} \Delta t \zeta Q_1^i.$$

370 Similarly, we solve Eq. (A1) using the same method. The channel cross-sectional area S is moved forward in time at all grid points by

$$S_j^{i+1} = S_j^i + \Delta t \left[\frac{(Q_j^i)^3}{(S_j^i)^{8/3}} \frac{1}{1 + \gamma(\hat{\theta}_j^i - \theta_i)} - S_j^i (N_j^i)^3 \right]$$

for $j = 1, 2, \dots, n$.

To evolve these two equations forward in time, the discharge and effective pressure at time step i is needed. These variables
375 can be found simultaneously solving the mass and momentum equations.

We follow Fowler (1999) and Kingslake (2013) in assuming ϵ is small enough to neglect the terms containing ϵ in Eq. (A2). With parameter values, $m_0, s_0 = 1000$ m, and $\rho_i = 917$ kg m⁻³, ϵ is on the order of 10^{-3} and thus we neglect these terms : **This-which** simplifies Eq. (A2) to

$$\frac{\partial Q}{\partial s} = 0. \tag{A9}$$

380 This is equivalent to assuming that any melt generated along the channel is small in comparison to the volume of fluid moving through the channel from the lake. Solving Eq. (A3) for the discharge Q and evaluating at the end of the channel gives

$$Q^2(\underline{s=1}, t) = \left(\delta \frac{\partial N}{\partial s}(\underline{s=1}, t) + \psi(\underline{s=1}, t) \right) S(\underline{s=1}, t)^{8/3}. \tag{A10}$$

From Eq. (A6) and the assumption that the discharge is always positive (flowing out of the lake), **we get**

$$Q(\underline{s=1}, t) = \sqrt{S(\underline{s=1}, t)^{8/3} \psi(\underline{s=1}, t)} \sqrt{S(1, t)^{8/3} \psi(1, t)}. \tag{A11}$$

385 From Eqs. (A11) and (A9), $Q(s, t) = Q(1, t)$ and we arrive at the following equation for discharge as a function of time

$$Q(t) = \sqrt{S(\underline{s=1}, t)^{8/3} \psi(\underline{s=1}, t)} \sqrt{S(1, t)^{8/3} \psi(1, t)}.$$

We solve this equation by calculating the discharge profile at each grid point by

$$Q_j^i = \sqrt{(S_n^i)^{8/3} \psi_n^i}. \tag{A12}$$

To calculate the effective pressure along the channel, we start with the boundary condition at the lake (**given in** Eq. (A5))
390 and use Eq. (A3) to iterate

$$N_{j+1}^i = N_j^i + \frac{\Delta s}{\delta} \left(\frac{(Q_j^i)^2}{(S_j^i)^{8/3}} - \psi_j^i \right) \tag{A13}$$

from $j = 1, 2, \dots, n$.

To solve the **simplified** dimensionless brine equation Eq. (A4), we use an upwind difference scheme such that

$$\hat{\beta}_j^{i+1} = \hat{\beta}_j^i - \Delta t \left[\frac{\beta_j^i}{S_j^i} \left(\frac{S_j^i - S_j^{i-1}}{\Delta t} \right) + \frac{Q_j^i}{\lambda S_j^i} \left(\frac{\hat{\beta}_j^i - \hat{\beta}_{j-1}^i}{\Delta s} \right) + \frac{\beta_j^i M}{\lambda S_j^i} \right].$$

395 After calculating the non-dimensional salt concentration, we re-dimensionalize the salt concentration to be in units of [kg m⁻³] and convert this **into psu using, to [psu] using,**

$$\beta_j^{i+1} = \frac{\hat{\beta}_j^{i+1} \hat{\beta}_0 1000}{\rho_{b_j}^i}. \quad (\text{A14})$$

Using the dimensional salt concentration **with units psu in [psu]** at time $i + 1$ and location j along the channel, the updated salinity-dependent melting point of the ice can be calculated using

400 $\hat{\theta}_j^{i+1} = \underline{-5.7505-5.81} \times 10^{-7} (\beta_j^{i+1})^3 \underline{-6.3992+1.24} \times 10^{-7-6} (\beta_j^{i+1})^2 - \underline{6.05176.05} \times 10^{-2} (\beta_j^{i+1}) - \underline{4.64087.45} \times 10^{-1-8} P_i,$

for $i = 1, 2, \dots, m$.

The density of brine can be updated **using the updated brine similarly with the new salt** concentration using Eq. 6. The basic hydraulic gradient is a function of brine density and can be updated using the new brine density.

405 ~~The system of equations are solved using a constant time step of approximately 3 seconds and a constant grid spacing of 20 m.~~

Author contributions. This publication is a direct result of AJ's Master's Thesis who was lead on all aspects of the research. AJ, SM, and MS conceived the study and contributed to the research. LB and MT helped with clarifications of the methods. All authors contributed to editing the paper.

Competing interests. The authors declare that they have no conflict of interest.

410 *Acknowledgements.* We thank Natalie Wolfenburger for providing equations for the density and melting point as functions of salinity using FREEZCHEM. We acknowledge Jack Dockery for the helpful discussions regarding the derivation of the salinity equation. We would also like to thank two anonymous reviewers for their comments which have improved this manuscript. MS and LB are supported by NASA award 80NSSC20K1134. SGM would like to acknowledge the support of NSF grant nos. 1813654, 2112085 and the Army Research Office (W911NF-19-1-0288).

415 References

- Badgeley, J. A., Pettit, E. C., Carr, C. G., Tulaczyk, S., Mikucki, J. A., Lyons, W. B., and Team, M. S.: An englacial hydrologic system of brine within a cold glacier: Blood Falls, McMurdo Dry Valleys, Antarctica, *J. Glaciol.*, 63, 387–400, <https://doi.org/10.1017/jog.2017.16>, 2017.
- Beecroft, I.: Sediment Transport During an Outburst from Glacier De Tsidjiore Nouve, Switzerland, 16–19 June 1981, *Journal of Glaciology*, 420 29, 185–190, <https://doi.org/10.3189/S0022143000005244>, 1983.
- Bell, R. E., Studinger, M., Shuman, C. A., Fahnestock, M. A., and Joughin, I.: Large subglacial lakes in East Antarctica at the onset of fast-flowing ice streams, *Nature*, 445, 904–907, <https://doi.org/10.1038/nature05554>, 2007.
- Carrivick, J. L. and Tweed, F. S.: A review of glacier outburst floods in Iceland and Greenland with a megafloods perspective, *Earth Sci. Rev.*, 196, 102 876, <https://doi.org/10.1016/j.earscirev.2019.102876>, 2019.
- 425 Chang, B., Consiglio, A. N., Lilley, D., Prasher, R., Rubinsky, B., Journaux, B., and Powell-Palm, M. J.: On the pressure dependence of salty aqueous eutectics, *Cell Reports Physical Science*, 3, 100 856, <https://doi.org/10.1016/j.xcrp.2022.100856>, 2022.
- Chikita, K.: The expansion mechanism of Himalayan supraglacial lakes: Observations and modelling, *Himalayan Journal of Sciences*, 2, 118–120, <https://doi.org/10.3126/hjs.v2i4.826>, 2004.
- Church, M.: Baffin Island Sandurs: a study of Arctic fluvial processes, *Geological Survey of Canada Bulletin*, 216, 430 <https://doi.org/10.1017/S001675680003630X>, 1972.
- Clarke, G. K. C.: Hydraulics of subglacial outburst floods: new insights from the Spring-Hutter formulation, *J. Glaciol.*, 49, 299–313, 2003.
- Cuffey, K. M. and Paterson, W. S. B.: *The physics of glaciers*, Elsevier, Amsterdam, 4 edn., 2010.
- Dubnick, A., Sharp, M., Danielson, B., Saidi-Mehrabad, A., and Barker, J.: Basal thermal regime affects the biogeochemistry of subglacial systems, *Biogeosciences*, 17, 963–977, <https://doi.org/10.5194/bg-17-963-2020>, 2020.
- 435 Evatt, G. W., Fowler, A. C., Clarke, C. D., and Hulton, N. R. J.: Subglacial floods beneath ice sheets, *Phil. Trans. R. Soc. A*, 365, 1769–1794, <https://doi.org/10.1098/rsta.2006.1798>, 2006.
- Flowers, G. E.: Hydrology and the future of the Greenland Ice Sheet, *Nature Communications*, 9, 2729, <https://doi.org/10.1038/s41467-018-05002-0>, 2018.
- Forte, E., Fratte, M. D., Azzaro, M., and Guglielmin, M.: Pressurized brines in continental Antarctica as a possible analogue of Mars, *Sci. Rep.*, 6, 33 158, <https://doi.org/10.1038/srep33158>, 2016.
- 440 Fowler, A. C.: Breaking the seal at Grimsvötn, Iceland, *J. Glaciol.*, 45, 506–516, <https://doi.org/10.3189/S0022143000001362>, 1999.
- Frederick, B. C., Young, D. A., Blankenship, D. D., Richter, T. G., Kempf, S. D., Ferraccioli, F., and Siegert, M. J.: Distribution of subglacial sediments across the Wilkes Subglacial Basin, East Antarctica, *Journal of Geophysical Research: Earth Surface*, 121, 790–813, <https://doi.org/10.1002/2015JF003760>, 2016.
- 445 Guan, M., Wright, N. G., and Sleigh, P. A.: Multiple effects of sediment transport and geomorphic processes within flood events: Modelling and understanding, *International Journal of Sediment Research*, 30, 371–381, <https://doi.org/10.1016/j.ijsrc.2014.12.001>, 2015.
- Hubbard, A., Lawson, W., Anderson, B., Hubbard, B., and Blatter, H.: Evidence for subglacial ponding across Taylor Glacier, Dry Valleys, Antarctica, *Ann. Glaciol.*, 39, 79–84, <https://doi.org/10.3189/172756404781813970>, 2004.
- Jenson, A., Amundson, J. M., Kingslake, J., and Hood, E.: Long-period variability in ice-dammed glacier outburst floods due to evolving catchment geometry, *The Cryosphere*, 16, 333–347, <https://doi.org/10.5194/tc-16-333-2022>, publisher: Copernicus GmbH, 2022.
- 450

- Jenson, A., Skidmore, M., Beem, L., Truffer, M., and McCalla, S.: Subglacial brine flow [code], <https://doi.org/10.5281/zenodo.7829316>, 2023.
- Keisling, B. A., Nielsen, L. T., Hvidberg, C. S., Nuterman, R., and DeConto, R. M.: Pliocene–Pleistocene megafloods as a mechanism for Greenlandic megacanyon formation, *Geology*, 48, 737–741, <https://doi.org/10.1130/G47253.1>, 2020.
- 455 Kingslake, J.: Modelling ice-dammed lake drainage, Ph.D. thesis, University of Sheffield, 2013.
- Kingslake, J.: Chaotic dynamics of a glaciohydraulic model, *J. Glaciol.*, 61, 493–502, <https://doi.org/10.3189/2015JoG14J208>, 2015.
- Kjeldsen, K. K., Mortensen, J., Bendtsen, J., Petersen, D., Lennert, K., and Rysgaard, S.: Ice-dammed lake drainage cools and raises surface salinities in a tidewater outlet glacier fjord, west Greenland, *J. Geophys. Res. Earth Surf.*, 119, 1310–1321, <https://doi.org/10.1002/2013JF003034>, 2014.
- 460 Knobel, R.: An introduction to the mathematical theory of waves, vol. 3, American Mathematical Soc., 2000.
- Larsen, I. and Lamb, M.: Progressive incision of the Channeled Scablands by outburst floods, *Nature*, 538, 229–232, <https://doi.org/10.1038/nature19817>, 2016.
- Lyons, W. B., Mikucki, J. A., German, L. A., Welch, K. A., Welch, S. A., Gardner, C. B., Tulaczyk, S. M., Pettit, E. C., Kowalski, J., and Dachwald, B.: The Geochemistry of Englacial Brine From Taylor Glacier, Antarctica, *Journal of Geophysical Research: Biogeosciences*, 465 124, 633–648, <https://doi.org/10.1029/2018JG004411>, 2019.
- Maizels, J.: Jokulhlaup deposits in proglacial areas, *Quaternary Science Reviews*, 16, 793–819, 1997.
- Meerhoff, E., Castro, L. R., Tapia, F. J., and Pérez-Santos, I.: Hydrographic and biological impacts of a glacial lake outburst flood (GLOF) in a Patagonian fjord, *Estuar. Coast.*, 42, 132–143, <https://doi.org/10.1007/s12237-018-0449-9>, 2019.
- Mikucki, J. A., Foreman, C. M., Sattler, B., Lyons, W. B., and C., P. J.: Geomicrobiology of Blood Falls: an iron-rich saline discharge at the 470 terminus of the Taylor Glacier, Antarctica, *Aquat Geochem*, 10, 199–220, <https://doi.org/10.1007/s10498-004-2259-x>, 2004.
- Mikucki, J. A., Auken, E., Tulaczyk, S., Virginia, R. A., Schamper, C., Sørensen, K. I., Doran, P. T., Dugan, H., and Foley, N.: Deep groundwater and potential subsurface habitats beneath an Antarctic dry valley, *Nature Communications*, 6, 6831, <https://doi.org/10.1038/ncomms7831>, 2015.
- Morlighem, M., Rignot, E., Mouginot, J., Seroussi, H., and Larour, E.: Deeply incised submarine glacial valleys beneath the Greenland ice 475 sheet, *Nature Geoscience*, 7, 418–422, <https://doi.org/10.1038/ngeo2167>, 2014.
- Neal, E.: Hydrology and Glacier-Lake Outburst Floods (1987–2004) and Water Quality (1998–2003) of the Taku River near Juneau, Alaska, USGS Scientific Investigations Report 2007-5027, 27 p., 2007.
- Nienow, P. W., Sole, A. J., Slater, D. A., and Cowton, T. R.: Recent Advances in Our Understanding of the Role of Meltwater in the Greenland Ice Sheet System, *Current Climate Change Reports*, 3, 330–344, <https://doi.org/10.1007/s40641-017-0083-9>, 2017.
- 480 Nye, J. F.: Water flow in glaciers: Jökulhlaups, tunnels and veins, *J. Glaciol.*, 17, 181–207, <https://doi.org/10.3189/S002214300001354X>, 1976.
- Old, G. H., Lawler, D. M., and Snorrason, A.: Discharge and suspended sediment dynamics during two jökulhlaups in the Skaftá river, Iceland, *Earth Surface Processes and Landforms*, 30, 1441–1460, <https://doi.org/10.1002/esp.1216>, 2005.
- Rothlisberger, H.: Water Pressure in Intra- and Subglacial Channels, *J. Glaciol.*, 11, 177–203, <https://doi.org/10.1017/S0022143000022188>, 485 1972.
- Russell, A. J., Roberts, M. J., Fay, H., Marren, P. M., Cassidy, N. J., Tweed, F. S., and Harris, T.: Icelandic jökulhlaup impacts: Implications for ice-sheet hydrology, sediment transfer and geomorphology, *Geomorphology*, 75, 33–64, <https://doi.org/10.1016/j.geomorph.2005.05.018>, 2006.

- Rutishauser, A., Blankenship, D. D., Sharp, M., Skidmore, M. L., Greenbaum, J. S., Grima, C., Schroeder, D. M., Dowdeswell, J. A.,
490 and Young, D. A.: Discovery of a hypersaline subglacial lake complex beneath Devon Ice Cap, Canadian Arctic, *Science Advances*, 4,
eaar4353, <https://doi.org/10.1126/sciadv.aar4353>, 2018.
- Rutishauser, A., Blankenship, D. D., Young, D. A., Wolfenbarger, N. S., Beem, L. H., Skidmore, M. L., Dubnick, A., and Criscitiello, A. S.:
Radar sounding survey over Devon Ice Cap indicates the potential for a diverse hypersaline subglacial hydrological environment, *The
Cryosphere*, 16, 379–395, <https://doi.org/10.5194/tc-16-379-2022>, 2022.
- 495 Scanlan, K. M., Buhl, D. P., and Blankenship, D. D.: Polarimetric Airborne Radar Sounding as an Approach to Characterizing Subglacial
Röthlisberger Channels, *IEEE Journal of Selected Topics in Applied Earth Observations and Remote Sensing*, 15, 4455–4467, 2022.
- Schoof, C.: An analysis of instabilities and limit cycles in glacier-dammed reservoirs, *Cryosphere*, 14, 3175–3194, <https://doi.org/10.5194/tc-14-3175-2020>, 2020.
- Seroussi, H., Nakayama, Y., Menemenlis, D., Larour, E., Morlighem, M., Rignot, E., and Khazendar, A.: Continued retreat of Thwaites
500 Glacier controlled by bed topography and ocean circulation, *Geophysical Research Letters*, 2017.
- Siegfried, M. R., Fricker, H. A., Carter, S. P., and Tulaczyk, S.: Episodic ice velocity fluctuations triggered by a subglacial flood in West
Antarctica, *Geophysical Research Letters*, 43, 2640–2648, <https://doi.org/10.1002/2016GL067758>, 2016.
- Snorrason, A., Jónsson, P., Pálsson, S., Árnason, S., Víkingsson, S., and Kaldal, I.: November 1996 jökulhlaup on Skeiðarársandur outwash
plain, Iceland, *Spec. Publ. Int. Assoc. Sedimentol.*, 32, 55–65, 2002.
- 505 Spring, U. and Hutter, K.: Numerical Studies of Jökulhlaups, *Cold Reg. Sci. Tech.*, 4, 227–244, 1981.
- Stearns, L. A., Smith, B. E., and Hamilton, G. S.: Increased flow speed on a large East Antarctic outlet glacier caused by subglacial floods,
Nature Geoscience, 1, 827–831, <https://doi.org/10.1038/ngeo356>, 2008.
- Trivedi, C. B., Lau, G. E., Grasby, S. E., Templeton, A. S., and Spear, J. R.: Low-Temperature Sulfidic-Ice Microbial Communities, Borup
Fiord Pass, Canadian High Arctic, *Frontiers in Microbiology*, 9, 1622, <https://doi.org/10.3389/fmicb.2018.01622>, 2018.
- 510 Vick-Majors, T. J., Michaud, A. B., Skidmore, M. L., Turetta, C., Barbante, C., Christner, B. C., Dore, J. E., Christianson, K., Mitchell,
A. C., Achberger, A. M., Mikucki, J. A., and Priscu, J. C.: Biogeochemical Connectivity Between Freshwater Ecosystems be-
neath the West Antarctic Ice Sheet and the Sub-Ice Marine Environment, *Global Biogeochemical Cycles*, 34, e2019GB006446,
<https://doi.org/10.1029/2019GB006446>, 2020.
- Walder, J. and Costa, J.: Outburst floods from glacier-dammed lakes: The effect of mode of lake drainage on flood magnitude, *Earth Surf.
515 Process. Landforms*, 21, 701–723, [https://doi.org/10.1002/\(SICI\)1096-9837\(199608\)21:8<701::AID-ESP615>3.0.CO;2-2](https://doi.org/10.1002/(SICI)1096-9837(199608)21:8<701::AID-ESP615>3.0.CO;2-2), 1996.
- Wolfenbarger, N. S., Fox-Powell, M. G., Buffo, J. J., Soderlund, K. M., and Blankenship, D. D.: Compositional Controls on the Distribution
of Brine in Europa’s Ice Shell, *Journal of Geophysical Research: Planets*, 127, e2022JE007305, <https://doi.org/10.1029/2022JE007305>,
2022.